

# Ground State Phases of the Doped 4-Leg $t$ - $J$ Ladder

Steven R. White<sup>1</sup> and D.J. Scalapino<sup>2</sup>

<sup>1</sup>*Department of Physics and Astronomy, University of California, Irvine, CA 92697*

<sup>2</sup>*Department of Physics, University of California, Santa Barbara, CA 93106*

(September 28, 2018)

## Abstract

Using density matrix renormalization group techniques, we have studied the ground state of the 4-leg  $t$ - $J$  ladder doped near half-filling. Depending upon  $J/t$  and the hole doping  $x$ , three types of ground state phases are found: (1) a phase containing  $d_{x^2-y^2}$  pairs; (2) a striped CDW domain-wall phase, and (3) a phase separated regime. A CDW domain-wall consists of fluctuating hole pairs and this phase has significant  $d_{x^2-y^2}$  pair field correlations.

PACS Numbers: 74.20.Mn, 71.10.Fd, 71.10.Pm

arXiv:cond-mat/9608138v1 28 Aug 1996

The observation of spin gaps [1,2] in the 2-leg  $\text{SrCu}_2\text{O}_3$  and 4-leg  $\text{La}_2\text{Cu}_2\text{O}_5$  ladder compounds and the recent report of superconductivity in a hole doped  $(\text{La,Sr,Ca})_{14}\text{Cu}_{24}\text{O}_{41}$  compound containing  $\text{CuO}_2$  chains and 2-leg  $\text{Cu}_2\text{O}_3$  ladders [3] has brought renewed interest in the properties of even-leg metal-oxide ladders. Here, making use of recently developed density matrix renormalization group (DMRG) techniques [4], we study the  $t$ - $J$  model of a 4-leg ladder for a range of  $J/t$  values and dopings near half-filling. For the doped 4-leg  $t$ - $J$  ladder we find three types of ground state phases: (1) a pair-gas phase containing  $d_{x^2-y^2}$  pairs; (2) a striped CDW domain wall phase, where each domain wall consists of four holes; and (3) a phase separated regime.

The Hamiltonian for the  $t$ - $J$  model is

$$\mathcal{H} = -t \sum_{\langle ij \rangle, s} P_G \left( c_{i,s}^\dagger c_{j,s} + c_{j,s}^\dagger c_{i,s} \right) P_G + J \sum_{\langle ij \rangle} \left( \vec{S}_i \cdot \vec{S}_j - \frac{1}{4} n_i n_j \right), \quad (1)$$

where  $c_{i,s}^\dagger$  and  $\vec{S}_i = c_{i,\alpha}^\dagger \vec{\sigma}_{\alpha\beta} c_{i,\beta}$  are electron creation and spin operators respectively,  $n_i$  is the occupation number operator,  $P_G$  is the Gutzwiller projection operator which excludes configurations with doubly occupied sites, and  $\langle ij \rangle$  denotes nearest neighbor sites. Here we report results for ladders with open boundary conditions for hole dopings of  $0 \leq x \leq 0.25$  and various  $J/t$  values. Our calculations for the 4-leg ladders were carried out using a DMRG method in which transformation matrices were stored and used to construct the initial state for each superblock diagonalization [5]. Of order  $10^3$  states were kept per block, and the final transformation matrices were used to calculate the ground state expectation values of the desired operators at the end of the calculation.

The types of ground state phases which we have found are illustrated in Fig. 1. The results shown in Fig. 1 are for a  $20 \times 4$  lattice with from 8 to 16 holes. These figures represent the most probable configuration of holes in the system, obtained by maximizing the ground state expectation value of a hole projection operator

$$P(l_1, l_2, \dots) = \prod_{i=1} p(l_i), \quad (2)$$

where  $p(l) = (1-n_{l\uparrow})(1-n_{l\downarrow})$  is the hole projection operator for the  $l^{\text{th}}$  lattice site. The results

shown in Fig. 1 were obtained by maximizing  $\langle P(l_1) \rangle$  over  $l_1$ , then maximizing  $\langle P(l_1, l_2) \rangle$  over  $l_2$  with fixed  $l_1$ , etc., until all the holes have been located. Although this procedure is not guaranteed to give the maximum of  $\langle P(l_1, l_2, \dots) \rangle$  over all  $\{l_i\}$ , we have not observed any cases in which it appears to fail. The positions of the holes are shown as the solid circles in Fig. 1.

These pictures of most-likely hole configurations are representative of the three phases we have found for dopings  $0 < x < 0.25$ , with  $0.25 < J/t < 3$ . Fig. 1(a) shows a gas of pairs, which occurs at low doping levels for a wide range of  $J/t$ , in this case  $x = 0.1$ ,  $J/t = 0.35$ . Domain-wall phases occur at somewhat higher doping levels, also for a wide range of  $J/t$ . Fig. 1(b) shows a domain-wall phase for  $J/t = 0.5$ ,  $x = 0.15$ , where the most probable hole configuration has holes along a diagonal. For smaller values of  $J/t$ , the most probable hole configuration consists of a zig-zag pattern along the two center chains, as shown in Fig. 1(c) for  $x = 0.15$ ,  $J/t = 0.25$ . We will refer to the domain walls of Fig. 1(b) and 1(c) as “transverse” (1,1) and “longitudinal” domain walls, respectively. Phase separation, as shown in Fig. 1(d), where the holes have all moved to either end of the ladder, occurs for  $J/t$  greater than about 1.5-1.9, in this case  $J/t = 2$ . Phase separation first manifests as an attraction between domain walls, and as an attraction between the ends of the ladder and the walls, as shown in the figure. For  $J/t \sim 3$ , the holes become closely packed at the ends of the ladder [6].

In order to obtain a clearer picture of the nature of the pair-gas and domain-wall phases, we have examined various local correlations. Figure 2(a) shows the probability of various hole configurations near the most likely configuration for the system shown in Fig. 1(a). The diameter of the dots is proportional to the probability of the last hole being on that site, when all the other hole positions are fixed. In this case the left-hand hole of the second pair from the left is allowed to vary. Although the maximum point shown in Fig. 1(a) has this pair as nearest neighbors, the probability of the last hole being on either the site above or below the maximum point is nearly as large. The results are consistent with Lanczos calculations for two holes on a periodic  $\sqrt{26} \times \sqrt{26}$  lattice, in which for  $J/t = 0.35$  the

holes are about 20% more likely to be found across a diagonal than on near-neighbor sites [7,8]. Figure 2(b) shows the expectation value of the kinetic energy on each bond when the location of all but one of the holes [the same hole as in (a)] has been specified by the projection operator.

The expectation value of  $\vec{S}_i \cdot \vec{S}_j$  near the paired holes in the two most likely configurations of Fig. 2(a) is shown in Fig. 2(c) and (d). In these plots, the width of the lines is proportional to the bond strength  $-\langle \vec{S}_i \cdot \vec{S}_j \rangle$ . In addition to showing the nearest-neighbor correlations, we show next-nearest neighbor correlations when both sites are adjacent to the same hole, but only when these correlations are antiferromagnetic,  $\langle \vec{S}_i \cdot \vec{S}_j \rangle < 0$ . Antiferromagnetic correlations coupling next-nearest neighbor sites across dynamic holes is an almost universal feature of the doped  $t$ - $J$  model [9], and presumably other doped antiferromagnets. These frustrating correlations develop in order to minimize the kinetic energy [9]. The strong diagonal singlet correlation crossing the hole pair in Fig. 2(d) is a striking example of this effect. The kinetic energy term strongly favors a singlet bond connecting these sites since for four of the eight hops available to the holes in this configuration, this bond becomes a nearest-neighbor exchange bond. This diagonal singlet is characteristic of a  $d_{x^2-y^2}$  pair [9].

A closer view of the domain walls in Figs. 1(b) and (c) is shown in Fig. 3. The probability of finding at a given site the fourth hole making up a transverse domain wall is shown in Fig. 3(a). This shows that while the (1,1) direction is favored, the domain wall is fluctuating strongly. At larger values of  $J/t$  (e.g.  $J/t \sim 1$ ) the (0,1) direction becomes favored. The expectation value of the exchange field  $\vec{S}_i \cdot \vec{S}_j$  for this wall is plotted in Fig. 3(b). A number of its features are similar to those of the hole pair in Fig. 2(d). In this case, instead of one diagonal singlet bond, three bonds are apparent. These diagonal singlets allow the wall to fluctuate strongly, reducing the kinetic energy. Holes bind in pairs in order to share frustrating bonds [9]. In a pair, however, there is still frustration present, since the diagonal singlet represents antiferromagnetic correlations between sites on the same sublattice. In a transverse domain wall, however, the undoped spin background is broken into two unconnected parts by the wall, eliminating the frustration. Application of

a staggered magnetic field to one end of the system (not shown) shows that the domain walls separate  $\pi$ -phase shifted regions with short-range antiferromagnetic spin correlations. However, the kinetic energy of the wall is not as low as that of two isolated pairs, making the walls unstable at low hole densities for moderate values of  $J/t$ .

The kinetic energy favors hole configurations that 1) avoid the edge sites, since the open boundary conditions act like hard walls, and 2) avoid nearest-neighbor hole positions, since the holes act like hard-core objects. However, these types of hole configurations are generally not favored by the exchange energy, leading to competition. At weak to moderate  $J/t$  values, the  $(\pm 1, 1)$  directions are favored for the domain wall largely because these hole configurations avoid nearest-neighbor hole configurations.

An example of this competition is seen in the most probable location of a pair in the pair-gas phase. For  $J/t = 0.5$ , pairs are found primarily on outer chains in order to form undoped two-leg ladder structures [9]. An undoped 2-leg ladder has a spin gap of order  $0.5 J$ , which is associated with both a rise in the spin excitations and a lowering of the “vacuum” ground-state energy of the 2-leg ladder [10]. Thus an undoped 2-leg ladder is a low-energy configuration. For  $J/t = 0.35$ , the tendency of the holes to avoid the edge sites is slightly stronger, and pairs are more likely to be found on the two middle chains, as shown in Figs. 1(a) and 2(a).

For smaller values of  $J/t$ , this tendency of the holes to avoid the edge sites affects the structure of a domain wall, and a longitudinal domain wall becomes more likely than a transverse domain wall. In Fig. 3(c) we show the exchange field near a longitudinal domain wall. Again, diagonal singlet correlations are present. In this case singlets are frustrating only near the ends of the wall.

So far we have characterized the phases of the  $t$ - $J$  model using the most probable hole configurations for typical systems. However, representing a system by a single hole configuration suggests that the holes are nearly static, which for small or moderate values of  $J/t$  is very far from the truth. Although with DMRG we can calculate  $\langle P(l_1, l_2, \dots) \rangle$  for any given configuration, the space of configurations is too large to study or portray directly.

An alternative representation of the system can be obtained by generating a set of configurations chosen randomly from the probability distribution  $\langle P \rangle$ . (Since  $P$  is a projection operator,  $\langle P \rangle$  is nonnegative.) To generate these “typical” configurations, we have used a simple classical Monte Carlo algorithm to wander randomly through hole configuration space according to the probability distribution  $\langle P \rangle$ , which is calculated using DMRG. This Monte Carlo calculation is done after the DMRG sweeps have finished, and after we have found the most probable hole configuration, which is used as the starting point of the Monte Carlo. At each Monte Carlo step, a hole is chosen at random, as well as one of the four directions  $(\pm 1, 0)$ ,  $(0, \pm 1)$ . If the move of that hole one step in the chosen direction is not possible (e.g. a hop onto a neighboring hole), the step is rejected. If the step is possible, it is accepted with Metropolis probability  $\min(1, \langle P' \rangle / \langle P \rangle)$ , where the DMRG transformation matrices are used to calculate  $\langle P' \rangle$ . This procedure is fast enough to allow several hundred Monte Carlo sweeps, which is enough to get a number of typical configurations.

In Fig. 4(a) we show 12 typical configurations for a  $14 \times 4$  system with 8 holes and  $J/t = 0.5$ . The first configuration in the upper left is the initial, most probable one, showing two transverse domain walls. Moving downward, successive configurations are separated by 240 Monte Carlo steps, enough to make them nearly uncorrelated. We see that in most of the configurations, there are no recognizable domain walls. From these configurations (and others not shown) the holes appear to make up a strongly correlated gas, made up of clusters of two, four, and sometimes three holes. It is not obvious from the figure that the wavefunction represented by these configurations should exhibit the charge density wave (CDW) structure expected from a set of domain walls.

In Fig. 4(b) we show the total average hole density per rung  $n_r(l)$  for the system shown in Fig. 4(a). We see that a strong CDW density variation is present, as one would expect from the maximum probability domain-wall pictures: the domain walls take up four rungs, and are separated by two rungs, which form a low-energy undoped two-leg ladder. These CDW domain-wall structures are subtle correlations built into the ground state wavefunction, and are difficult to see in a limited number of hole-configuration snapshots, as in Fig. 4(a). The

density variations are usually commensurate with the lattice, with pronounced two-rung low-doping regions separating hole-rich domain-wall regions. The lattice sizes and dopings shown have been chosen to match and enhance these commensurate density variations. It is not clear from the results we have so far whether there is commensurate long-range CDW order at special fillings (such as  $x = 1/6$ ), or simply power-law decay of CDW correlations. Also shown in Fig. 4(b) are results for a  $24 \times 4$  system with  $J/t = 0.35$  and 6 holes, showing CDW correlations. In this case there are three separate pairs which give rise to these “ $4k_F$ ” CDW correlations, as opposed to the two-pair (4 hole) domain-wall structures of Fig. 1(b). This behavior in the pair-gas phase is similar to the pairing-CDW correlations observed in 2-chain ladders [11].

In Fig. 4(c) we show results for the equal-time  $d_{x^2-y^2}$  pair-field correlation function,  $D(l) = \langle \Delta_d(i) \Delta_d^\dagger(i+l) \rangle$ , where  $\Delta_d(i)$  destroys a nearest-neighbor  $d_{x^2-y^2}$  pair at site  $i$  [9]. The figure shows  $D(l=10)$  as a function of doping  $x$ , with  $i_x$  and  $i_x+l_x$  chosen symmetrically about the center of the lattice, and with  $i_y = i_y+l_y = 2$ . This quantity is useful as a measure of the overall strength of the pairing correlations. The pairing correlations for  $J/t = 0.5$  initially rise with doping, reaching a maximum between  $x = 0.15$  and  $x = 0.20$ , and then decrease. Extended  $s$ -wave pairing correlations (not shown) are much smaller in magnitude. For  $J/t = 0.5$  the magnitude of the correlations near the maximum is similar to that seen in a two-leg Hubbard ladder with  $U = 8t$  (corresponding to  $J \sim 4t^2/U = 0.5$ ) [11]. For  $J/t = 0.35$  the peak is reduced in magnitude and occurs at somewhat reduced doping. For  $J/t = 0.25$  the correlations (not shown) are less than  $10^{-4}$ . The behavior of  $D(l)$  versus  $l$  near the maximum (not shown) is consistent with a power law behavior. The results shown bear a strong resemblance to a plot of  $T_c$  versus  $x$  for a typical cuprate superconductor [12]. Remarkably, the pairing correlations are larger in the domain-wall phase than in the pair-gas phase. The domain-wall phase appears to exhibit “supersolid” behavior, with simultaneous pairing and CDW correlations. From the hole-configuration snapshots, we see how this can happen: the domain walls appear as an unbound resonance of hole pairs. There are also weaker resonances involving three-hole structures. These resonances are not strong enough

to significantly weaken the pairing, and, in fact, the increased density of pairs in the domain-wall phase leads to an increase in the pairing correlations relative to the more dilute pair-gas phase, as seen in Fig. 4(c).

The domain-wall phase we have found resembles in some respects the singlet striped phase proposed by Tsunetsugu, et. al. [10] In addition, various Hartree-Fock calculations [13–16], as well as Gutzwiller variational Monte Carlo calculations [17] have found evidence for the formation of domain walls in the 2D Hubbard model. The possibility that a CDW domain-wall phase occurs prior to phase separation was suggested by Prelovsek and Zotos [7] based on studies of four-hole correlation functions on small  $t$ - $J$  clusters. Our present calculations show that domain-wall CDW ground state phases can occur in 4-leg  $t$ - $J$  ladders. The domain walls should be thought of as highly-fluctuating resonances of pairs. These CDW domain-wall phases have significant  $d_{x^2-y^2}$  pair field correlations, which are substantially stronger than in the low-doping pair-gas phase.

#### ACKNOWLEDGEMENTS

We would like to thank S.A. Kivelson and T.M. Rice for useful discussions. SRW acknowledges support from the NSF under Grant No. DMR-9509945, and DJS acknowledges support from the Department of Energy under grand DE-FG03-85ER45197, and from the Program on Correlated Electrons at the Center for Material Science at Los Alamos National Laboratory.

## REFERENCES

- [1] K. Kojima, et. al., Phys. Rev. Lett. **74**, 2812 (1995).
- [2] B. Batlogg, et. al., Bull. Am. Phys. Soc. **40**, 327 (1995).
- [3] M. Uehara, T. Nagata, J. Akimitsu, H. Takahashi, N. Mori, and K. Kinoshita, preprint.
- [4] S.R. White, Phys. Rev. Lett. **69**, 2863 (1992), Phys. Rev. B **48**, 10345 (1993).
- [5] S.R. White, 1996 preprint, cond-mat/9604129.
- [6] For large values of  $J/t$ , DMRG can become stuck in metastable hole-cluster configurations, such as all in a cluster at one end rather than split into two clusters at the ends. To find the lowest energy state, one can initialize the DMRG iterations with the holes forced into specific locations, allow convergence, and then choose the calculation with the lowest final energy.
- [7] P. Prelovsek and X. Zotos, Phys. Rev. B **47**, 5984 (1993).
- [8] D. Poilblanc, Phys. Rev. B **49**, 1477 (1994).
- [9] S. R. White and D.J. Scalapino, preprint, cond-mat/9605143.
- [10] H. Tsunetsugu, M. Troyer, and T.M. Rice, Phys. Rev. B **51**, 16456 (1995).
- [11] R.M. Noack, S.R. White, and D.J. Scalapino, Phys. Rev. Lett. **73**, 882 (1994).
- [12] B. Keimer, et. al. Phys. Rev. B **46**, 14034 (1992).
- [13] H.J. Schulz, Journal de Physique, **50**, 2833 (1989).
- [14] D. Poilblanc and T.M. Rice, Phys. Rev. B **39**, 9749 (1989).
- [15] J. Zaanen and O. Gunnarsson, Phys. Rev. B **40**, 7391 (1989).
- [16] Verges, J.A., et. al., Phys. Rev. B **43**, 6099 (1991).
- [17] T. Giamarchi and C. Lhuillier J.A., Phys. Rev. B **42**, 10641 (1990).

## FIGURES

FIG. 1. Maximum likelihood hole configurations obtained by maximizing the expectation value of  $P(\ell_1, \ell_2, \dots)$ , Eq. (2), illustrating the three phases of the doped 4-leg  $t$ - $J$  ladder. (a) A gas of pairs with  $J/t = 0.35$  and a filling of  $x = 0.1$ . (b) “Transverse” (1,1) domain walls with  $J/t = 0.5$  and  $x = 0.15$ . (c) “Longitudinal” domain walls with  $J/t = 0.25$  and  $x = 0.15$ . (d) Phase separation with  $J/t = 2.0$  and  $x = 0.2$ .

FIG. 2. This sequence of plots shows a section of the lattice for the pair-gas phase, Fig. 1(a), with  $J/t = 0.35$  and  $x = 0.1$ , containing the second pair from the left. (a) The probability of finding the second member of a hole pair when the first has been projected out at the gray shaded position. All of the holes in other pairs have also been projected out. The diameter of the black dots is proportional to the probability of finding the hole on the corresponding site. (b) The hopping kinetic energy of one member of a pair when the other is projected out at the shaded site, shown as the width of the line connecting nearest neighbor sites, according to the scale shown. (c) The expectation value of  $\vec{S}_i \cdot \vec{S}_j$  between various sites when the holes are nearest neighbors and (d) when they are next nearest neighbors.

FIG. 3. A section of a  $20 \times 4$  lattice showing a domain wall, with  $J/t = 0.5$  and  $x = 0.15$ , as in Fig. 1(b). (a) The probability of finding the fourth hole when the others have been projected out, and (b) the expectation value of  $\vec{S}_i \cdot \vec{S}_j$  when all holes have been projected out in their most likely configuration. (c) Same as (b), but for the system shown in Fig. 1(c), with  $J/t = 0.25$ .

FIG. 4. (a) Typical hole configurations of a  $14 \times 4$  lattice with  $J/t = 0.5$ , and 8 holes. (b) The total average hole density on a rung as a function of the rung location. The upper curve is for the system shown in (a). The lower curve is for a  $24 \times 4$  system with  $J/t = 0.35$  and 6 holes. (c) The equal time  $d_{x^2-y^2}$  pair field correlation function  $D(l)$  at a separation of  $l = 10$  rungs versus doping  $x$ , for  $20 \times 4$  and  $16 \times 4$  systems and  $J/t = 0.35$  and  $0.5$ . The number of holes in each of the systems shown is a multiple of four.

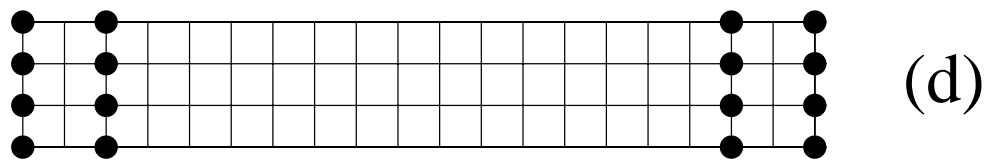
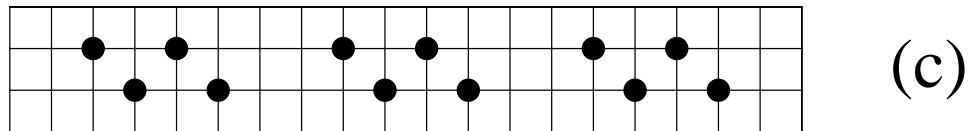
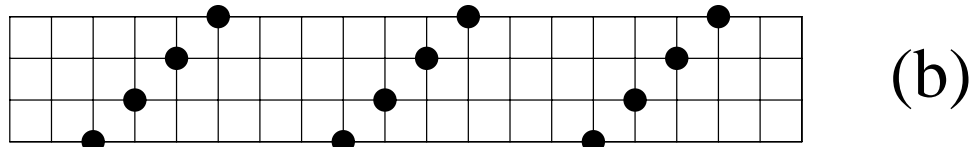
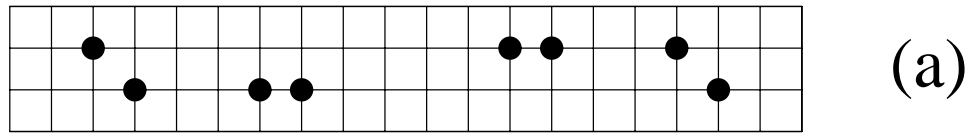


Fig. 1  
White and Scalapino

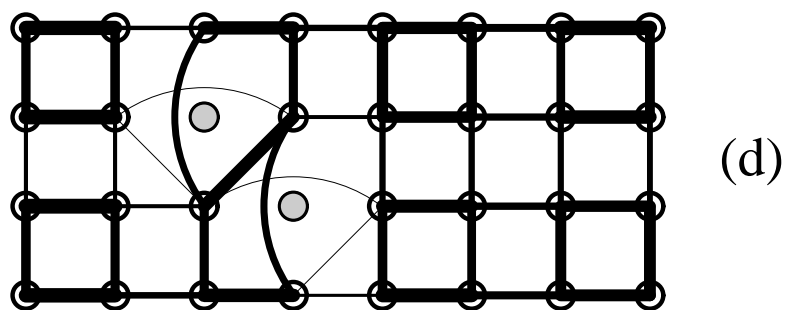
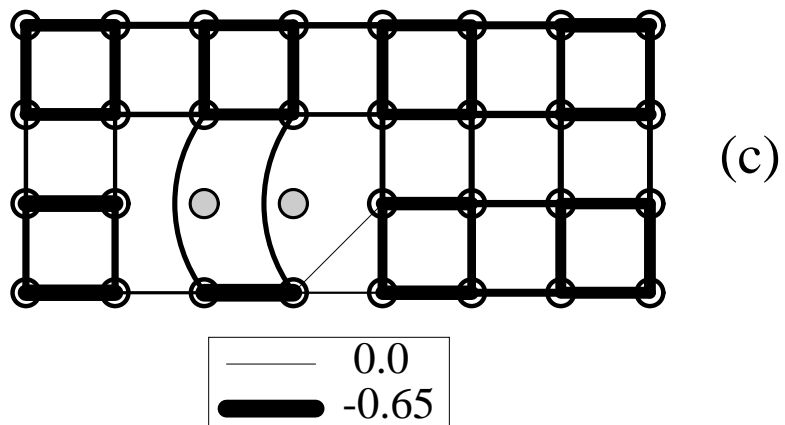
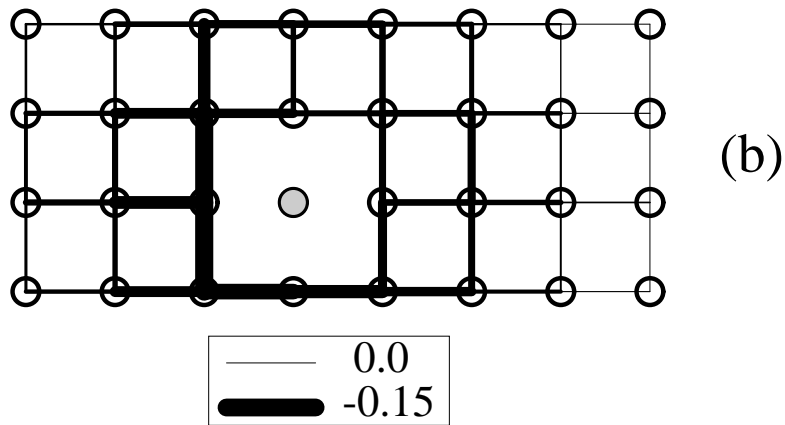
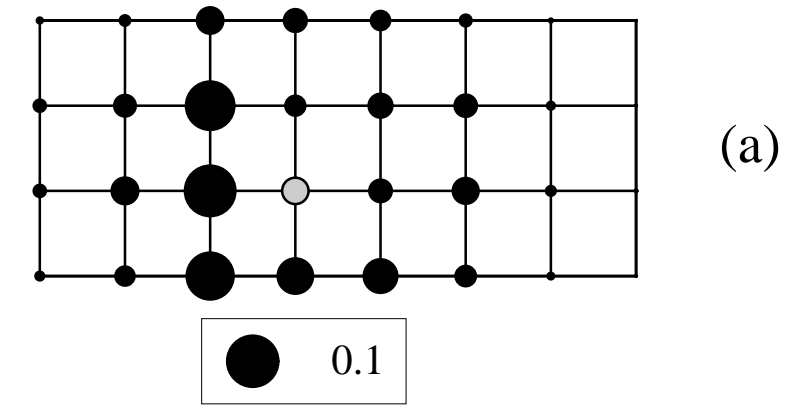
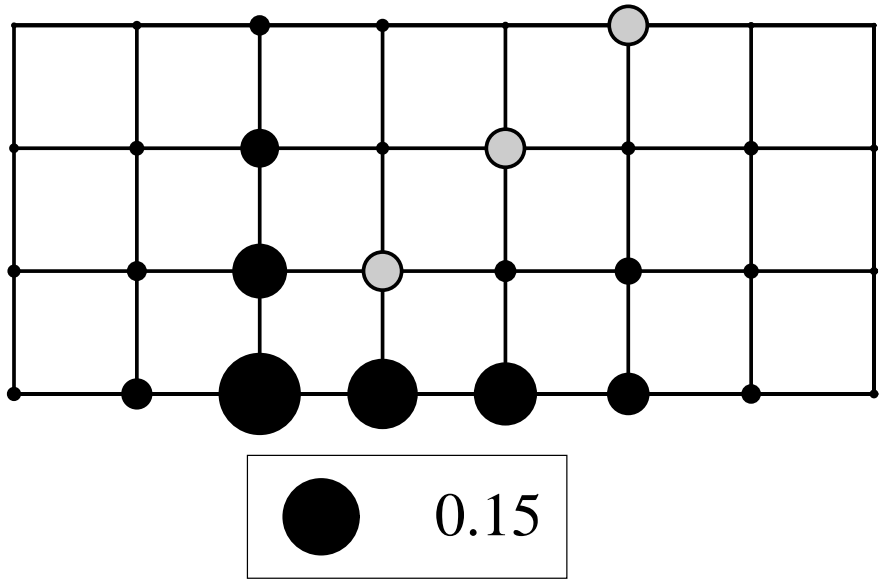
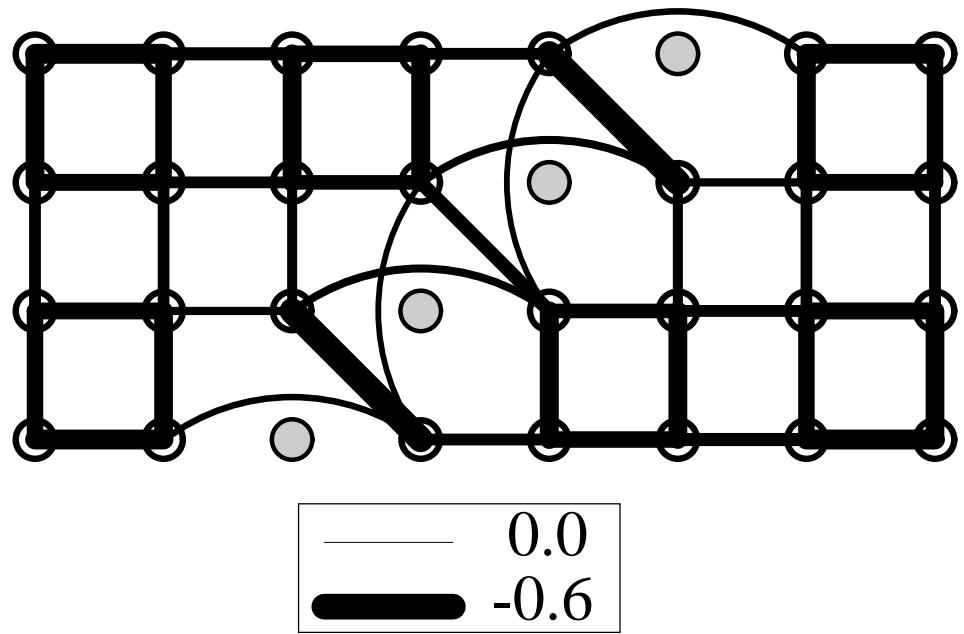


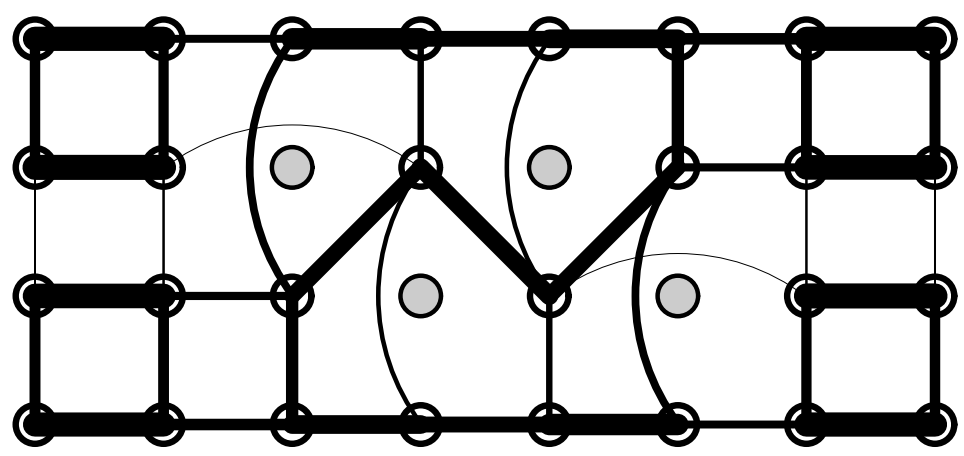
Fig. 2  
 White and Scalapino



(a)



(b)



(c)

Fig. 3  
White and Scalapino

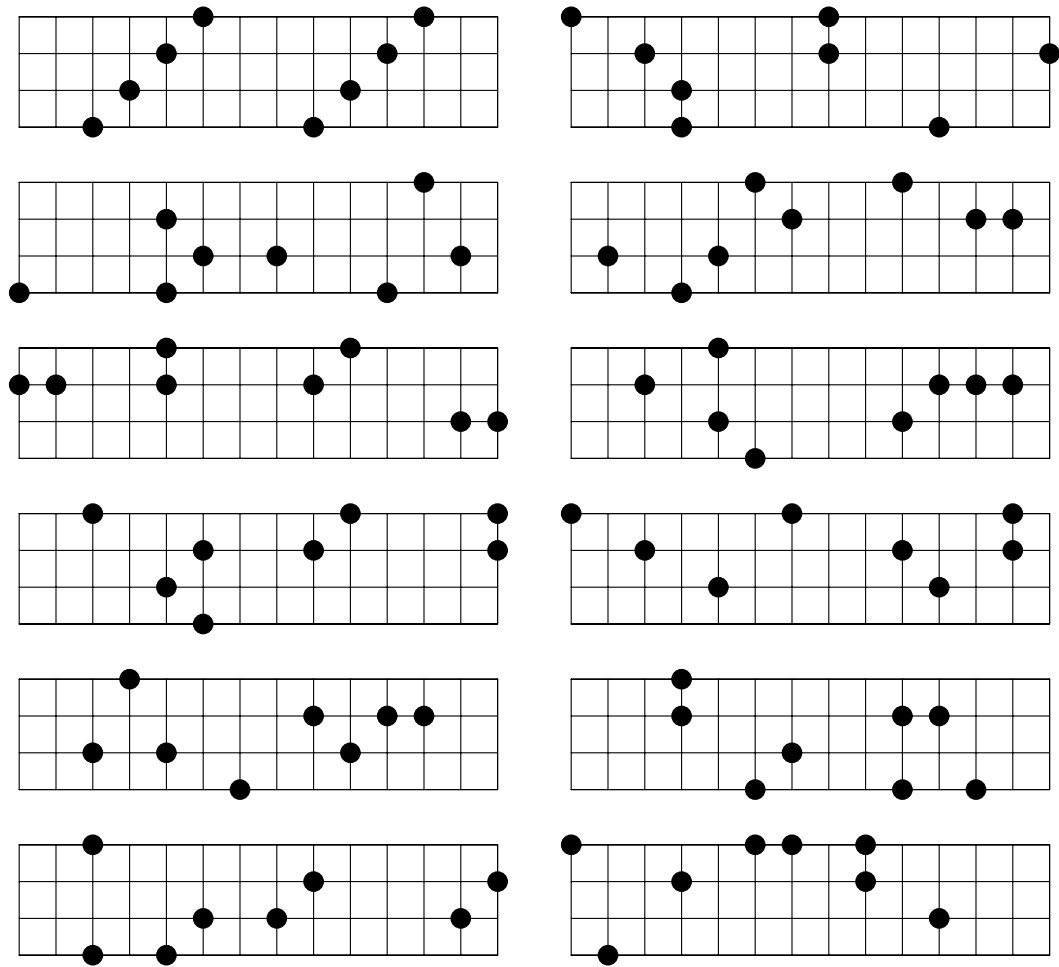


Fig. 4(a)  
White and Scalapino

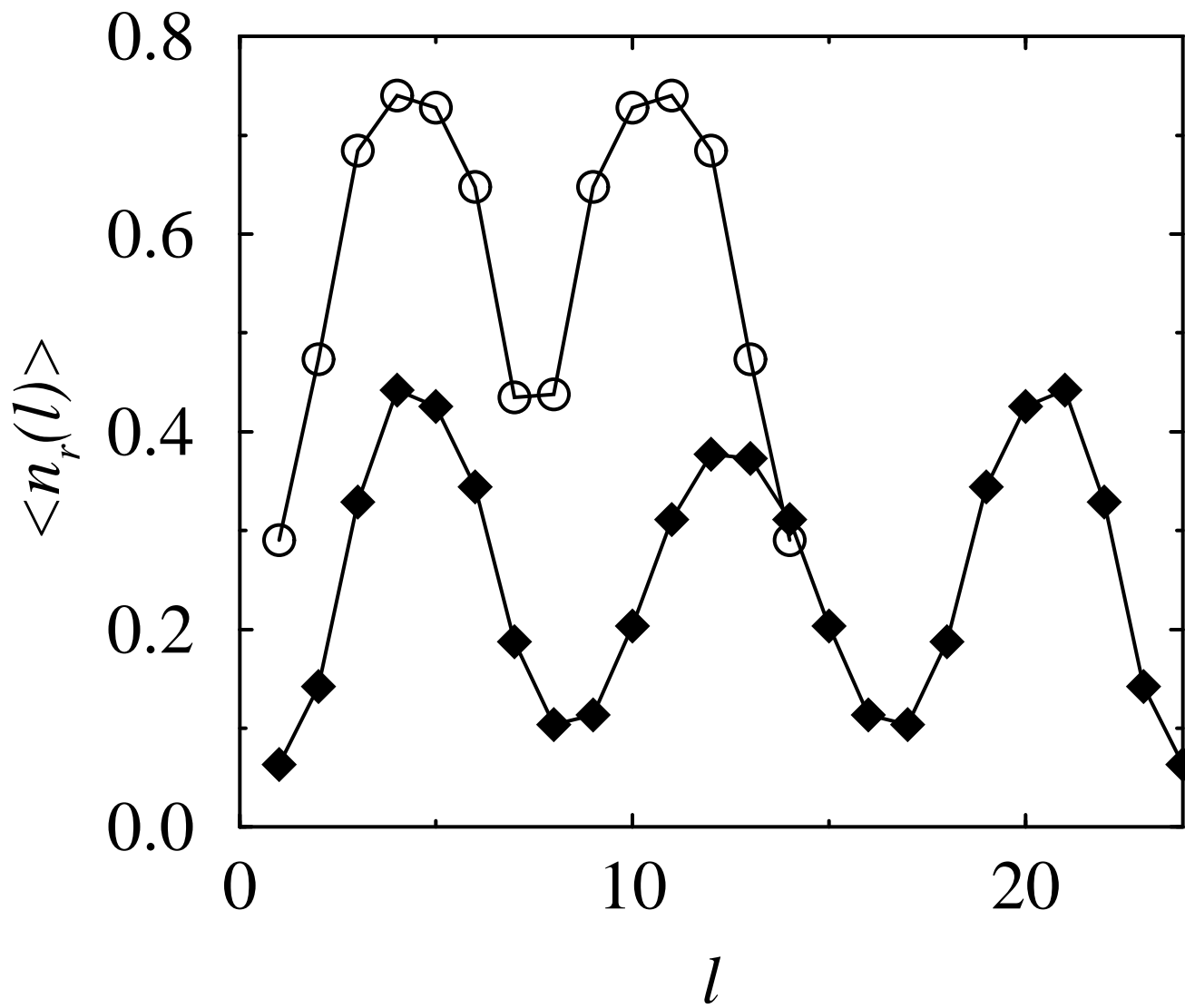


Fig. 4(b)  
White and Scalapino

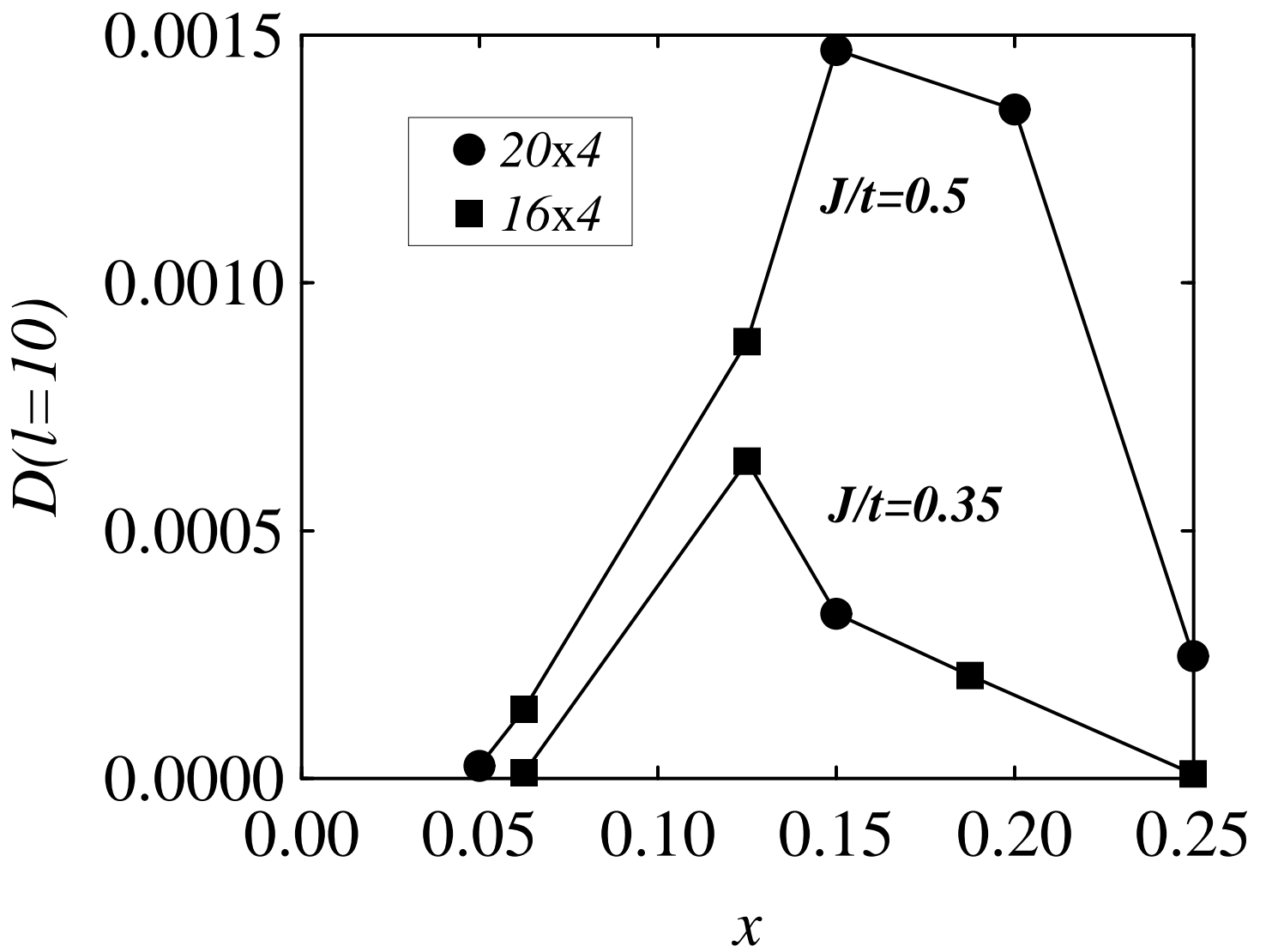


Fig. 4(c)  
White and Scalapino